Friction Estimation for Railway Brake Systems in Field Tests

Schwarz, Christoph[1], Lüdicke, Daniel[1] and Heckmann, Benjamin[2]

[1]Institute of System Dynamics and Control, German Aerospace Center (DLR)
[2]Knorr-Bremse Rail Vehicle Systems

Abstract

Condition based monitoring concepts for railway brake systems offer a row of promising advantages: improved safety, reduced noise emission, and economic benefits by an optimal utilization of every single brake unit. However, a reliable determination of the current state of the brake components is difficult due to the rough operating conditions and the economic effort of a direct, optical identification. To ease the conflict between the economic restrictions, the required accuracy of the information, and the robustness of the measurement equipment, the current work presents a model-based observer design. This observer estimates the friction coefficients between brake disc and brake calipers for every wheelset of a train. To enable a railway-compliant and economically reasonable implementation, the observer configuration relies on a set of robust sensors, which are mostly used in modern trains. Furthermore, the influence of the train resistance on the longitudinal dynamics is taken into account to minimize the disturbance in the evaluation of the actual brake friction coefficients. In a next step the information on these friction coefficients can be used to display a maintenance alarm for not properly working brake equipment.

Keywords: Model-based estimation; brake monitoring; friction identification

1 Introduction

Every engineering discipline that deals with safety and comfort issues is usually engaged in the field of condition monitoring [13]. Since safety and comfort are highly relevant for the operation of railway vehicles, there was, is, and probably will be a lot of research on this topic in the railway engineering community. The monitoring techniques are divided into wayside and on-board techniques [1]. Furthermore, in [17] the techniques are classified into signal processing, knowledge-based, and model-based methods. The model-based methods can be split up into parameter estimation, parity equation, and state observer methods. The authors in [3], [5], and [17] presented some essential benefits of model-based, on-board monitoring applications with a focus on suspension components and the wheel-rail interface.

Also for railway brake systems the application of monitoring techniques offers some significant advantages. Firstly, shorter brake distances and reduced noise emissions can be achieved by an optimal condition of the brake components. Secondly, the economic benefits by an optimal utilization of every single brake unit have to be mentioned. As a concrete example the approach presented in [4] describes a monitoring concept for the braking control based on accelerometer and gyro measurements. However, the accelerometer related monitoring is not able to locate effects of single brake units. The works [1] and [9] deal with brake pad inspection systems using digital image processing and machine vision technology to identify wear rates and uneven wear as well as to detect missing brake pads. These optical methods use either infrared technology to unveil hot spots or they process non-thermographic images to determine cracks and other superficial damages. The sensibility of the optical sensors and the economic effort have to be named as major drawbacks of these approaches.

To alleviate the described weaknesses the current work presents a model-based, on-board observer design for the friction behavior of railway brake units. The presented approach is characterized by its generic setup in combination with the reliable estimation of the friction conditions for every single wheelset of a train. Therefore, Section 2 presents the considered dynamics as well as the translation into an observer prediction model. The relevant details of the executed field tests, i.e. the vehicle configuration and the track properties, are described in Section 3. Section 4 illustrates significant results before Section 5 draws a conclusion and denotes the upcoming tasks.

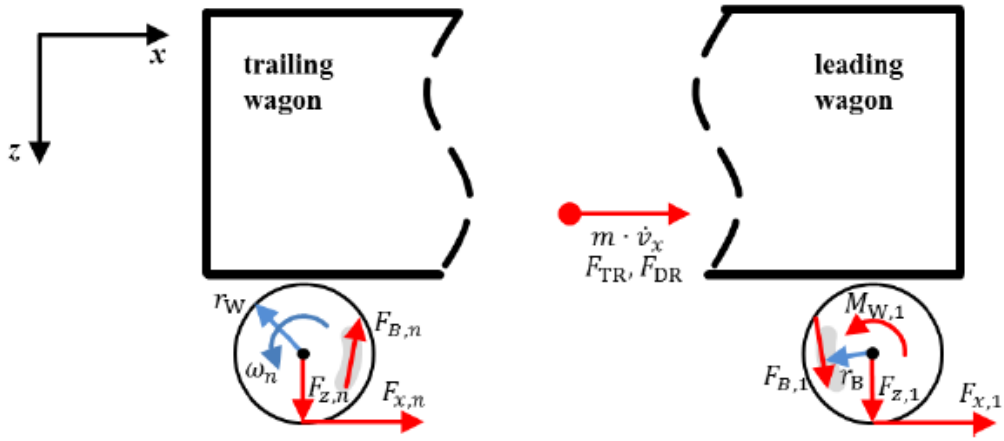

Figure 1: *Scheme of the train model with forces, torques and kinematic quantities*

2 Estimator Synthesis

The following section describes a generic system configuration of a train together with the modeling of the friction characteristics. The focus of the second part is on the determination of the train and track related resistance forces and torques. At the end of this chapter, the observer prediction model is defined and the most important aspects of the parameter estimator theory are denoted.

2.1 System Definition

The work in [15] shows that a plane 2D model of a wheelset, which neglects lateral dynamics, is well suited to identify the friction and longitudinal dynamics during braking. Extending these assumptions to a whole train with multiple wheelsets leads to the concept shown in Figure 1, where the relevant forces and torques are depicted in red and the kinematic quantities in blue. The interrelations between forces, torques and further dynamics are described in Equations (1) to (4). The parameters and variables used therein are listed in Table 1. To set up the dynamic system, moment equilibria around the lateral axis of each wheelset and the longitudinal force equilibrium of the entire train are stated. According to Figure 1 the moment equilibrium of one wheelset is

$$J_{y,i} \cdot \dot{\omega}_i = n_{B,i} \cdot F_{B,i} \cdot r_B + 2F_{x,i} \cdot r_W + M_{W,i}. \quad (1)$$

Table 1: *Parameters (left) and variables (right) of the 2D train system*

n	number of wheelsets	ω_i	wheelset rotational velocity
i	wheelset specifying index $[1,\ldots,n]$	v_x	longitudinal train velocity
r_{W}	wheel radius	$F_{x,i}$	longitudinal wheel-rail creep force
r_{B}	friction radius	$F_{\mathrm{B},i}$	friction force of the brake unit
m	mass of the train	$F_{z,i}$	wheelset load
$J_{y,i}$	wheelset inertia	$M_{\mathrm{W},i}$	additional wheel torques
$n_{\mathrm{B},i}$	number of brakes per wheelset	F_{TR}	track resistance force
$F_{\mathrm{S},i}$	slack adjuster force	F_{DR}	drag resistance force
η_i	efficiency of the brake rigging	$p_{c,i}$	brake cylinder pressure
A_i	piston surface	$\mu_{\mathrm{B},i}$	brake coefficient of friction
$i_{\mathrm{B},i}$	brake rigging ratio	$\mu_{\mathrm{W},i}$	wheel-rail coefficient of friction

The additional wheel torques $M_{W;\mathrm{i}}$ comprise for example the electro-dynamic brake torque as well as rolling and bearing resistances. The force equilibrium in longitudinal direction that considers the train as one single rigid body reads

$$m \cdot \dot{v}_x = F_{\mathrm{TR}} + F_{\mathrm{DR}} + \sum_i 2F_{x,i}. \tag{2}$$

Concentrating all the wagon masses in one body provides a good trade-off between sufficient accuracy and reasonable computational effort. The calculation of the track and drag resistance forces, F_{TR} and F_{DR}, is described in section 2.2. For the modeling of the friction behavior in the brake unit exist different approaches, e.g. [10]. These methods take a row of different influences into account, for example the material combination, the temperatures of disc and caliper and the relative velocity between them. Nevertheless, there usually are unknown environmental disturbances like water and dirt and, in addition, the parameters of these models vary for different brakes. Due to this lack of a simple but generally valid formula the friction coefficients $\mu_{B;i}$ are assumed to be constant in this work and the brake force reads

$$F_{\mathrm{B},i}(t) = \mu_{\mathrm{B},i} \cdot \eta_i \cdot i_{\mathrm{B},i} \cdot (p_{c,i}(t) \cdot A_i - F_{\mathrm{S},i}), \quad \text{with} \quad \dot{\mu}_{\mathrm{B},i} = 0,. \tag{3}$$

It has to be mentioned that the time-invariant modeling of $\mu_{B;i}$ does not affect the time-variant behavior of the later on described estimator.

The same motivation that is stated for the modeling of the dynamics of $\mu_{B;i}$ holds for

Table 2: *System parameters and variables of the observer prediction model*

r_{BR}	bearing radius	μ_{BR}	bearing friction coefficient
c_{d}	drag coefficient	e_{RR}	longitudinal contact point shift
A_{d}	drag area	ρ	mass density of air

the wheel-rail interface. There are well proven theories, e.g. [12], [7], that describe the friction dynamics for different environmental conditions. However, the actual environmental influences in daily train operation cannot be reasonably identified. Therefore, it is more suitable in the present context to implement again a constant friction behaviour

$$F_{x,i}(t) = \mu_{\mathrm{W},i} \cdot \frac{F_{z,i}(t)}{2}, \quad \text{with} \quad \dot{\mu}_{\mathrm{W},i} = 0, \tag{4}$$

and adapt the friction coefficient by the observer.

2.2 Train and Track Resistance

The observer shall take the influence of the train and track resistances on the longitudinal dynamics into account. In this way it is intended to achieve an accurate evaluation of the actual friction coefficients with a minimized amount of superposed disturbances. The resistances are divided into the train related and the track related effects, which are both described in the following. The train resistances include the rolling and bearing resistance torques, M_{RR} and M_{BR}, as well as the drag force F_{DR}, cf. [14]

$$\begin{aligned} M_{\mathrm{BR}} &= r_{\mathrm{W}} \cdot F_{z,i} \cdot f_{\mathrm{BR}}, \quad \text{with} \quad f_{\mathrm{BR}} = \frac{1}{\sqrt{\frac{r_{\mathrm{W}}^2}{\mu_{\mathrm{BR}}^2 \cdot r_{\mathrm{BR}}^2}\left(1+\mu_{\mathrm{BR}}^2\right)-1}} \\ M_{\mathrm{RR}} &= e_{\mathrm{RR}} \cdot F_{z,i}, \\ F_{\mathrm{DR}} &= c_{\mathrm{d}} \cdot A_{\mathrm{d}} \frac{\rho}{2} \cdot v_x^2. \end{aligned} \tag{5}$$

Table 2 lists the parameters of Equation (5) and of the track resistance calculation in the next paragraph. The starting resistance caused by the not yet existent oil film in the bearings is neglected, since the focus is on the braking not the accelerating process.

To identify the track resistance forces F_{CR} (curvature resistance) and F_{SR} (slope resistance) the horizontal and vertical track characteristics are determined in this paragraph. The horizontal course is generally constructed by a sequence of routing elements (straight lines, curves and transitional curves). The curvature κ as a characteristic parameter of the horizontal routing is defined as

$$\kappa = \frac{\Delta\phi}{\Delta s}, \tag{6}$$

with the heading angle ϕ and the travel length s. According to [14] the curvature resistance acting on the train is

$$F_{\mathrm{CR}} = f \cdot m \cdot g, \quad \text{with} \quad f = \kappa\,(0.158 \cdot a + 0.033 \cdot b)\,. \tag{7}$$

The empirical coefficient *f* depends on the wheel base a and the wheel gauge *b*.

The vertical course is defined by straight lines of different pitch, which are linked by parabolas at the line intersection points (tangent cuts). In this way a continuous height profile is generated. As the characteristic parameter of vertical routing the slope angle β

$$\tan(\beta) = \frac{\Delta z}{\Delta s} \tag{8}$$

is used with height *z*. The gradient resistance acts via the up- or downhill force

$$F_{\mathrm{SR}} = m \cdot g \cdot \sin(\beta)\,. \tag{9}$$

The distance basis Δs in (6) and (8) affects the signal to noise ratio. This allows for a geometric low pass filtering in distance domain, see Section 3.2. In the end, the described resistance effects are combined with the dynamic setup of Section 2.1 to synthesize the observer in the next subsection.

2.3 Parameter Estimator Design

As the observer is implemented to estimate the friction conditions, the state vector

$$\boldsymbol{x} = [v_x, \omega_1, \ldots, \omega_n, \mu_{\mathrm{B},1}, \ldots, \mu_{\mathrm{B},n}, \mu_{\mathrm{W},1}, \ldots, \mu_{\mathrm{W},n}]^T \in \mathbb{R}^{3\cdot n+1} \tag{10}$$

contains not only the kinematic velocities v_x and ω_i but also the friction coefficients $\mu B;I$ and $\mu_{W;i}$. In consequence, the nonlinear state space representation

$$\dot{\boldsymbol{x}} = \boldsymbol{f}(\boldsymbol{x},\boldsymbol{u}) + \boldsymbol{q}, \quad \boldsymbol{y} = \boldsymbol{C}\boldsymbol{x} + \boldsymbol{r} \tag{11}$$

merges the differential equations and dynamic definitions of Equations (1) to (5). The output equation is linear with the output matrix $\mathbf{C} = [\mathbf{I}_{\mathrm{n+1\times n+1}} \quad \mathbf{0}_{\mathrm{n+1\times 2\cdot n}}]$, i.e. the states v_x and themselves are defined as measurement signals **y**. Furthermore, the input vector

$$\boldsymbol{u} = [p_{c,1}, \ldots, p_{c,n}, F_{\mathrm{TR}}]^T \in \mathbb{R}^{n+1} \tag{12}$$

includes the brake cylinder pressures $p_{c;i}$ and the track resistance force F_{TR}. Considering F_{TR} as input offers the advantage that its determination described in the foregone section can be changed to a cloud-based track information service without adapting the observer environment. The terms ***q*** and ***r*** denote the process and the measurement noise, which are assumed to be zero-mean and Gaussian distributed: ***q***~N (0;***Q***), r~N (0;***R***).

Due to the nonlinear characteristic of (11) the Extended Kalman Filter (EKF), a wellestablished observer concept for nonlinear systems, is chosen. Basically, the EKF is divided into a prediction and a correction step, which consider the tuning covariance matrices $\boldsymbol{Q}$ and $\boldsymbol{R}$, respectively. For a detailed discussion of nonlinear filter methods the interested reader is referred to [16]. The time-discrete observer algorithm used in this work is based on the implementation presented in [2]. The reliability and robustness in the railway context was validated in [15] for a roller rig environment.

3 Field Test Environment

The first part of this chapter highlights the relevant aspects of the test vehicle and the measurement equipment. The second part illustrates the peculiarities of the test scenario.

3.1 Vehicle Configuration

The realization of the above described observer concept is done for a two-part diesel multiple unit with standard gauge. This train of the Siemens Desiro Classic family is operated by the German Erzgebirgsbahn [6]. It is equipped with motor bogies at the

Table 3: *Parameters of the test vehicle*

	wheelset load	wheelset inertia J_y	wheel base a
MB front wheelset	13.4 t	96 kg·m^2	1.9 m
MB rear wheelset	14.1 t	126 kg·m^2	
JTB	14.5 t	209 kg·m^2	2.65 m

front (MB 1) and rear end (MB 2) and a Jacobs trailer bogie (JTB) in the middle. The wheelset rotations in both MBs are mechanically coupled, so that the train has got only four independent wheelset rotations. The distance l between the bogie pivots is 16 m and the nominal wheel radius r_W is 0.38 m. Regarding the brake equipment the MBs are identical but they are not symmetrically by themselves, i.e. one wheelset has got one axle brake unit and the other wheelset has got two axle brake units. Due to this peculiarity and the mounting of the motor an unbalanced mass distribution between the two wheelsets of the MBs is assumed, see Table 3. The JTB wheelsets have got two wheel brake units.

Regarding the measurement equipment it has to be mentioned that the set of sensors is specifically designed for the field tests. However, the measurements of the wheelset rotational speeds ωi and the brake pressures $p_{c;i}$ build the basis for the observer. Usually, these signals are detected in trains with a wheel slide protection system anyway. In addition, a slip-free measurement of the longitudinal speed v_x is realized by an optical sensor.

After the specification of the necessary equipment for the parameter estimator, the sensors that are used for the identification of the track characteristics are denoted. The longitudinal and lateral accelerations, a_x and a_y, are both recorded by four sensor sets that are distributed along the train chassis. Using the mean value of multiple acceleration sensors provides an improved accuracy, since the influence of measurement noise is reduced. Anyhow, the lateral movement could not be calculated using the a_y sensors, since these sensors only measure the partial lateral acceleration of the inclined car body due to the superelevated track.

Another sensor is the two-frequency GNSS sensor with a GNSS antenna on the vehicle roof. This sensor provides the position signal via longitude and latitude coordinates of WGS84 reference ellipsoid and the altitude via the height above the ellipsoid surface. For a better processing of the GNSS position signal it is transformed into a local NED (north east down) coordinate system [8]. This is a two-step process, which starts with the trans-

Table 4: *Test scenario parameters*

	case 1	case 2	case 3	case 4	case 5	case 6
$v_0 \left[\frac{\text{km}}{\text{h}}\right]$	65	78	77	115	81	85
direction	fw	bw	fw	bw	fw	fw
type	FSB	FSB	FSB	EB	EB	EB

formation of the angular position (latitude, longitude, altitude (LLA)) into the geocentric Cartesian coordinate system ECEF (earth-centered earth-fixed) of WGS84 datum. In the second step the ECEF coordinates are transformed to a local NED coordinate system. To minimize the deviation between the curved surface of the WGS84 reference ellipsoid and the plane Cartesian coordinate system, the base of the NED coordinate system might be placed in the middle of the scheduled track.

Finally, the motion signals along the track (s_x, v_x, a_x) are generated by a sensor fusion of the speed, acceleration, and GNSS sensors. Thus, the horizontal and vertical gradients between two positions in the NED coordinate system define the current heading angle ($\Delta\phi$) and height deviations (Δz). The positioning accuracy might be further enhanced by the inclusion of angular velocities from gyroscopes or inertial measurement units (IMU). The results of the track characterization according to Equations (6) and (8) that are received with the presented set of sensors are described in the next subsection.

3.2 Test Scenarios

There are six test cases investigated, which are carried out in Germany in the area around Zwickau, Chemnitz, and Aue. The brake scenarios include emergency (EB) and full ser-

vice brake (FSB) applications to verify the observer functionality under extreme conditions. Furthermore, the initial velocity v_0 before starting the braking process is varied between 65 $\frac{km}{h}$ and 115 $\frac{km}{h}$ and the tests are executed in both directions (forward: fw, backward: bw). Table 4 lists the combinations of the six scenarios. In the considered test cases only the friction brakes are used with a maximum brake pressure $p_{c;i}$ of 2 bar for the JTB brake units and 3.4 bar for the MB brake units.

Figure 2 (left) shows a map with the calculated track of case 6 in blue. The middle of the test track is at the LLA-coordinates (50.5976°, 12.6939°, 342.043m) what corresponds to the ECEF-coordinates ($3.95777632 \cdot 10^6$m, $8.91479549 \cdot 10^5$m, $4.90551675 \cdot 10^6$m).

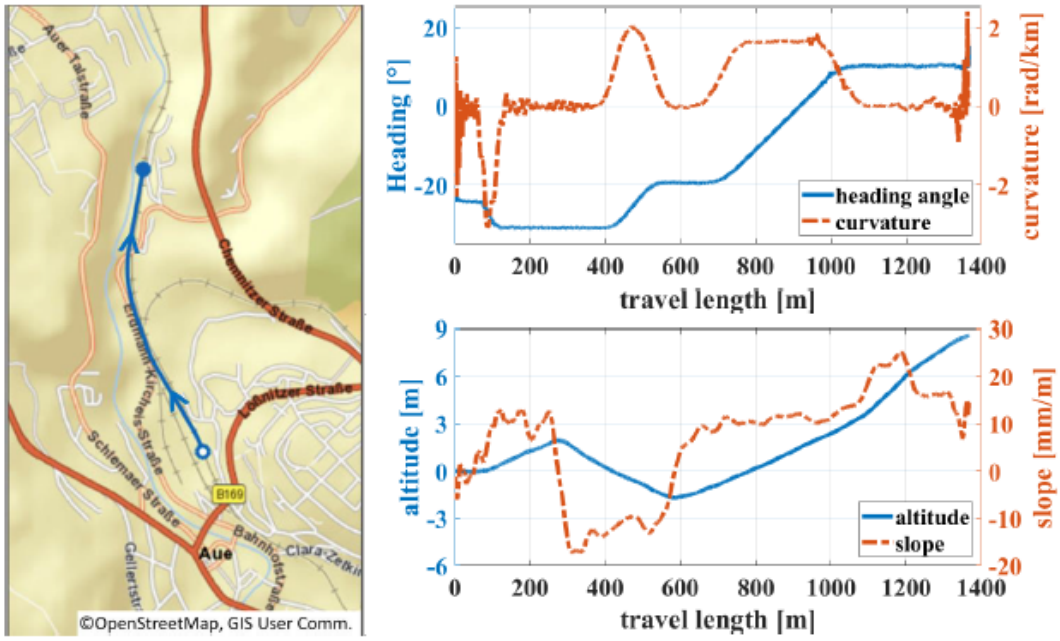

Figure 2: *(left) Map of the test area in case 6 and calculated track in blue, (top right) calculated heading and curvature, and (bottom right) calculated altitude and slope*

Starting at the southern end of the blue line the train passes a switch and after a short, straight section two right curves hook up. The vertical track characteristic is determined by three slope changes, which occur due to the location in the German Central Uplands. The two plots on the right of Figure 2 illustrate the calculation results of curvature and slope according to Section 2.2. All in all, the single track segments are clearly identified and the results verify a sufficient accuracy regarding the presented use case. Minor disturbances in the form of high-frequency oscillations in the curvature arise at the beginning and the end of the scenario but they do not measurably degrade the estimation results. In this first and last test section the geometric low pass filtering, mentioned in Section 2.2, is not fully able to cancel out the noise in the positioning data. The slope results show a similar oscillating behavior but with a lower amplitude and frequency, so that they can

be rated as sufficiently accurate as well. In Figure 3 the velocity of the train is illustrated. The profile is characterized by two accelerating phases (0-20s and approximately 38-70s) and the braking phase from t = 80s to the full stop at t = 102s. Using this track and velocity information the friction estimator is parametrized and tested in the next section.

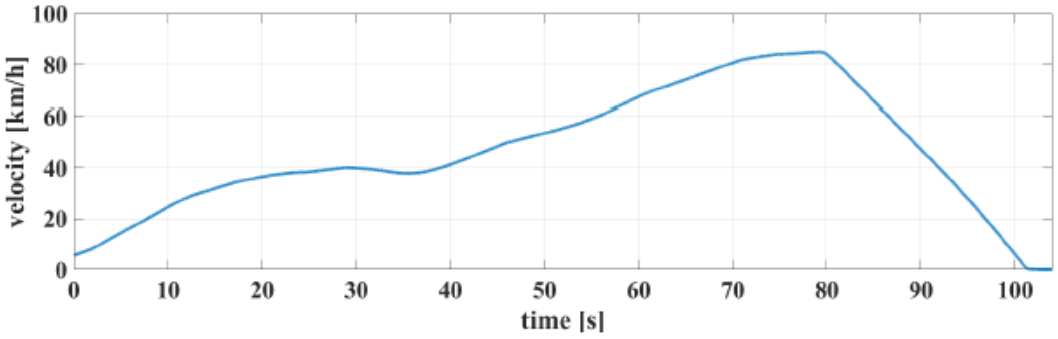

Figure 3: *Velocity profile of the test drive*

4 Results and Discussion

As mentioned in Section 2.3 the observer estimates the dynamics depending on the covariance matrices $\boldsymbol{R}$ and $\boldsymbol{Q}$. To find the optimal parameters for these positive definite matrices a multi-case optimization is set up, see [11]. Consequently, there are twelve independent tuning parameters referring to the diagonal entries of $\boldsymbol{R}$ and $\boldsymbol{Q}$

$$\boldsymbol{R} = diag\left(\boldsymbol{R}_v, \boldsymbol{R}_{\omega,1}, \boldsymbol{R}_{\omega,2}, \boldsymbol{R}_{\omega,3}, \boldsymbol{R}_{\omega,4}\right) \tag{13}$$
$$\boldsymbol{Q} = diag\left(\boldsymbol{Q}_v, \boldsymbol{Q}_{\omega,1}, \boldsymbol{Q}_{\omega,2}, \boldsymbol{Q}_{\omega,3}, \boldsymbol{Q}_{\omega,4}, \boldsymbol{Q}_{\mu_B}, \boldsymbol{Q}_{\mu_B}, \boldsymbol{Q}_{\mu_B}, \boldsymbol{Q}_{\mu_B}, \boldsymbol{Q}_{\mu_W}, \boldsymbol{Q}_{\mu_W}, \boldsymbol{Q}_{\mu_W}, \boldsymbol{Q}_{\mu_W}\right).$$

For the sake of a limited complexity of the optimization only one $\boldsymbol{Q}_{\mu B}$ and one $\boldsymbol{Q}_{\mu W}$ are defined, to represent the assumably identical covariances of the friction characteristics. The objective function O is defined as the maximum of the case objective functions O_c

$$O = \max_c\left(O_c\right), \tag{14}$$
$$O_c = \frac{1}{t_{\mathrm{end},c}} \int_0^{t_{\mathrm{end},c}} \boldsymbol{w}_\omega \cdot |\Delta\boldsymbol{\omega}| + w_v \cdot |\Delta v_x| \, \mathrm{d}t,$$

with c = 1, ..., 5 representing the case and $t_{end;c}$ the case duration. The parameters $\boldsymbol{w}_\omega$ and w_v weight the absolute deviations between measured and observed velocities. Using the maximum of all *Oc* ensures that a configuration is determined, which is supposed to be robust and performs well in every application scenario. Case 6 is used to test the observer in a not specifically optimized scenario, what is presented in the next paragraph.

Figure 4 shows the measurements of case 6 that are provided for the observer. The results of MB 2 and the second JTB wheelset are left out, as they are hardly distinguishable from the presented results.

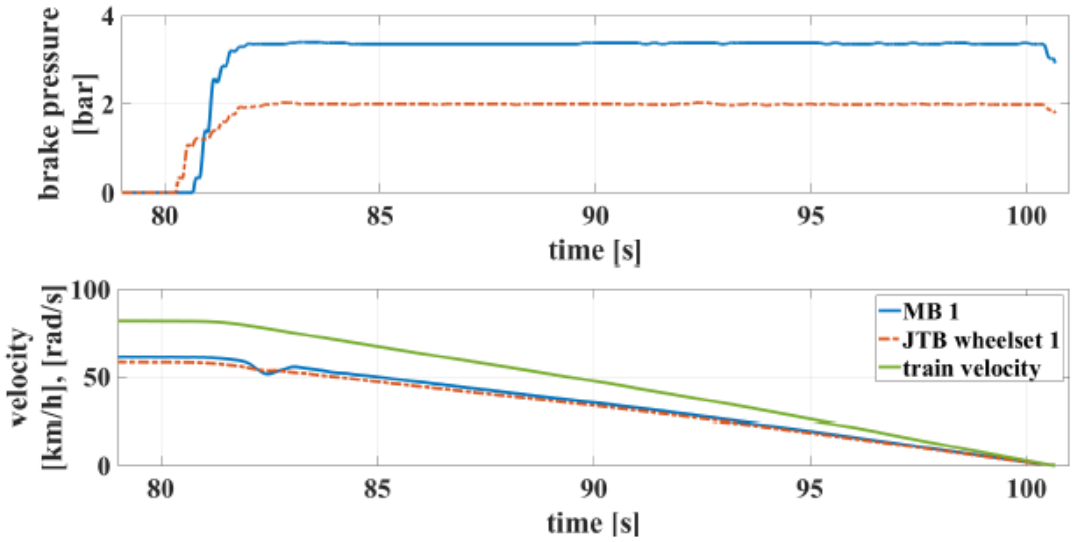

Figure 4: *Measurement information provided to the observer*

The upper part depicts the brake cylinder pressures. Since the JTB wheelsets are equipped with two wheel brake units, their pressure level is lower than for the MB wheelsets with 1 and 2 axle brake units, respectively. The lower plot illustrates the translational train velocity as well as the rotational wheelset velocities. The velocity of MB 1 shows a short phase of critical overbraking at t ≈ 82s.

The acceleration, velocity, and brake distance results of the observer reveal an almost ideal estimation. This might be obvious, as all the velocity measurements are included in the observer input. Regarding the friction results it has to be mentioned that the estimated $\mu_{B;i}$ and $\mu_{W;i}$ of single wheelsets cannot be quantitatively validated, since there is no information on the actual friction coefficients. Nevertheless, the mean value of the friction estimations is confirmed with respect to the measured train acceleration and brake distance. Furthermore, the results in Figure 5 validate the friction behavior at least in a qualitative way and the plausibility could be verified on an experience base.

On the left hand side the normalized friction coefficients of the brake units are plotted, which clearly denote the trend of an increasing friction induced by a rising brake disc and pad temperature. The difference between the JTB and MB results might be caused by the dependence of the friction coefficients on the normal force (and in consequence on the brake pressure) between brake disc and pad, see [10]. The major oscillation at t = 81s coincides with the first contact between brake pad/disc and it describes a settling process that is common for most observer methods. In the further process only minor short-term oscillations occur, which do not severely diminish the overall reliability.

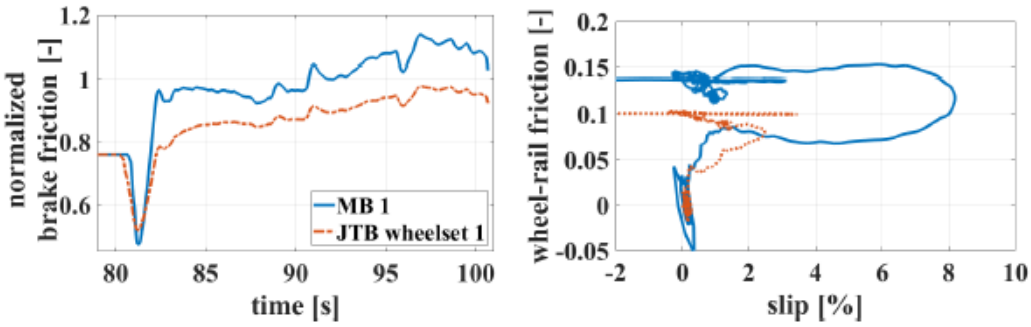

Figure 5: *Brake friction (left) and wheel-rail friction (right) estimation*

The plot on the right of Figure 5 illustrates the wheel-rail friction $\mu_{W;1}$ of MB 1 over the estimated slip. The two levels of $\mu_{W;1}$ at 0.07 and 0.15 occur due to a short track section with slippery conditions. This low adhesion phase is the reason for the overbraking in Figure 4 at t ≈ 82s. Since the leading MB 1 cleans up the rails, the following wheelsets do not show this distinct overbraking behavior. The fact that $\mu_{W;2}$ is smaller than $\mu_{W;1}$ might have two reasons, see Equation (4). Firstly, $F_{z;2}$ is larger than $F_{z;1}$ according to the higher wheelset load of the JTB wheelset, see Table 3. Secondly, $F_{x;2}$ is smaller than $F_{x;1}$, since the brake pressure as well as brake friction of MB 1 are higher. All in all, the results demonstrate a robust and reliable performance of the friction estimator.

5 Conclusions and Outlook

The presented work illustrates the design process for a friction estimator as a first step to a condition-based monitoring concept. First of all, the online calculation of train and track resistances and the implementation of a generic observer prediction model are described. The designed observer requires measurement data of the angular wheelset velocities, the longitudinal train speed and the brake cylinder pressures. Regarding the track identification the longitudinal acceleration of the train and its positioning data have to be recorded. The fact that most of these sensors are already in use in modern trains enables a railway-compliant and economic reasonable implementation. In the end, the presented estimation results validate the reliability and robustness of the observer for the given test cases. One of the upcoming tasks is to evaluate long-term field test data, so that a correct identification of the friction degradation can be verified. In addition, these long-term results allow for the setup and testing of a condition-based monitoring concept for the brakes. Finally, the combination with a cloud-based communication will allow to use the estimated friction data of an entire train fleet and to build up a self-learning monitoring environment.

Acknowledgements

This work was partially funded by StMWi (StMWi grant number: MST-1308-0006//BAY 191/002), the Bavarian Ministry of Economic Affairs and Media, Energy and Technology, within the project DynORail. The WGS84 transformation is based on the software IFSSimulationsumgebung developed by Dr. Daniel Lüdicke during his employment at the Institute of Rail Vehicles and Transport Systems of RWTH Aachen University.

References

[1] Barke, D. and Chiu, W.K. Structural health monitoring in the railway industry: A review. Structural Health Monitoring, 4(1):81–94, 2005.

[2] Brembeck, J., Pfeiffer, A., Fleps-Dezasse, M., Otter, M.,Wernersson, K., and Elmqvist, H. Nonlinear state estimation with an extended FMI 2.0 co-simulation interface. In Proceedings of the 10th International Modelica Conference, pages 53–62, Lund, Sweden, 2014. Linköping University Electronic Press.

[3] Bruni, S., Goodall, R.M., Mei T.X., and Tsunashima, H. Control and monitoring for railway vehicle dynamics. Vehicle System Dynamics, 45(7-8):743–779, 2007.

[4] Charles, G. and Goodall, R.M. Low adhesion estimation. In 2006 IET International Conference on Railway Condition Monitoring, pages 96–101, Birmingham, UK, 2006. The Institution of Engineering and Technology.

[5] Charles, G., Goodall, R.M., and Dixon, R. Model-based condition monitoring at the wheel-rail interface. Vehicle System Dynamics, 46(sup1):415–430, 2008.

[6] DB RegioNetz Verkehrs GmbH / Infrastruktur GmbH Erzgebirgsbahn. VT 642, June 2019. https://www.erzgebirgsbahn.de/erzgebirgsbahn/view/wir/vt_642.shtml. [7] Kalker, J.J. Three-Dimensional Elastic Bodies in Rolling Contact. Kluwer Academic Publishers, Dordrecht, The Netherlands, 1st edition, 1990.

[8] Lüdicke, D. Schienenfahrzeug- und Umgebungssimulation mit absolutem Raumund Zeitbezug. Dissertation, RWTH Aachen University, 2018.

[9] Ngigi, R., Pislaru, C., Ball, A., and Gu, F. Modern techniques for condition monitoring of railway vehicle dynamics. Journal of Physics: Conference Series, 364:012016, 2012.

[10] Ostermeyer, G.P. On the dynamics of the friction coefficient. Wear, 254(9):852–858, 2003.

[11] Pfeiffer, A. Optimization library for interactive multi-criteria optimization tasks. In Proceedings of the 9th International Modelica Conference, pages 669–680, Munich, Germany, 2012. Linköping University Electronic Press.

[12] Polach, O. A fast wheel-rail forces calculation computer code. Vehicle System Dynamics, 33(sup1):728–739, 1999.

[13] Rao, B.K.N., editor. Handbook of condition monitoring. Elsevier Advanced Technology, Oxford, UK, 1st edition, 1996.

[14] Schindler, C., editor. Handbuch Schienenfahrzeuge-Entwicklung, Produktion, Instandhaltung. DVV Media Group GmbH, Hamburg, 1st edition, 2014.

[15] Schwarz, C., Brembeck, J., and Heckmann, B. Dynamics observer for the longitudinal behavior of a wheelset on a roller rig. Proceedings of the Institution of Mechanical Engineers, Part F: Journal of Rail and Rapid Transit, 233(10):1112–1119, 2019.

[16] Simon, D. Optimal State Estimation: Kalman, H Infinity, and Nonlinear Approaches. Wiley & Sons, Hoboken, New Jersey, 1st edition, 2006.

[17] Strano, S. and Terzo, M. Review on model-based methods for on-board condition monitoring in railway vehicle dynamics. Advances in Mechanical Engineering, 11(2):1–10, 2019.

Autoren

Schwarz, Christoph

B.Sc. and M.Sc. degrees in Mechanical Engineering from Technical University of Munich (TUM), Germany. Since 2014 Research Assistant at the Institute of System Dynamics and Control of the German Aerospace Center (DLR).

Address: Münchener Straße 20, 82234 Wessling, Germany.

E-Mail: christoph.schwarz@dlr.de

Lüdicke, Daniel

Diplom degree in Mechatronics from Technical University of Ilmenau, Germany. From 2009 to 2014 Research Assistant at the Institute for Rail Vehicles and Transport Systems of RWTH Aachen University. PhD degree on the topic of vehicle automation and advanced odometry with satellite navigation in 2018. Since 2016 he works at the Institute of System Dynamics and Control of the German Aerospace Center (DLR).

Address: Münchener Straße 20, 82234 Wessling, Germany.

E-Mail: daniel.luedicke@dlr.de

Heckmann, Benjamin

Diplom degree in Mechanical Engineering from Technical University of Munich (TUM), Germany. From 2007 to 2013 Research Assistant at the Institute of Applied Mechanics of TUM. Since 2013 he works as System Engineer at the Knorr-Bremse Rail Vehicle Systems GmbH.

Address: Moosacher Straße 80, 80809 Munich, Germany.

E-Mail: benjamin.heckmann@knorr-bremse.com